C h a p t e r 5

Efficient Synthesis of Narrowly Dispersed Brush Copolymers and Study of Their Assembly

Portions of this chapter have been published: Xia, Y.; Olsen, B. D.; Kornfield, J. A.; Grubbs, R. H. *J. Am. Chem. Soc.* **2009**, *131*, 18525.

Abstract

Efficient, one-pot preparation of synthetically challenging, high molecular weight (MW), narrowly dispersed brush block copolymers and random copolymers in high conversions was achieved by ring-opening metathesis (co)polymerization (ROMP) of various macromonomers (MMs) using the highly active, fast-initiating ruthenium olefin metathesis catalyst $(H_2IMes)(pyr)_2(Cl)_2RuCHPh$. A series of random and block copolymers were prepared from a pair of MMs containing polylactide (PLA) and poly(*n*-butyl acrylate) (P*n*BA) side chains at similar MWs. Their self-assembly in the melt state was studied by small angle X-ray scattering (SAXS) and atomic force microscopy (AFM). In brush random copolymers containing approximately equal volume fractions of PLA and P*n*BA, the side chains segregate into lamellae with domain spacing of 14 nm as measured by SAXS, which was in good agreement with the lamellar thickness measured by AFM. The domain spacings and order-disorder transition temperatures of brush random copolymers were insensitive to the backbone length. In contrast, brush block copolymers containing approximately equal volume fractions of these MMs self-assembled into highly-ordered lamellae with domain spacing over 100 nm, making the assembly structures photonic crystals.

Introduction

Brush polymers possess an interesting extended conformation due to the high steric crowding from high density sides chains, as discussed in Chapter 4.[1] Their nonspherical macromolecular geometries and lengths up to a few hundred nanometers afforded numerous potential applications in nanoscience, such as molecular actuators,[2] templates for inorganic particles,[3-5] and as precursors for nanocapsules[6], nanotubes[7], and other carbon nanostructures[8].

On the other hand, linear block copolymers have proven to be versatile, powerful tools in the "bottom-up" approach to create nanostructured materials with novel mechanical, optical, and electronic properties and with specific functionalities over the last few decades.[9] When two or more different types of side chains are attached to a linear polymer backbone to form brush copolymers, each side chain may behave like a block segment in a block copolymer: they can be long enough to drive segregation, due to selective solubility or enthalpically favored demixing, yet are constrained by covalent attachment onto a single molecule. The spatial arrangement of different types of side chains along the backbone and their relative ratio should dramatically affect the assembly of the copolymers. The assembly of brush copolymers may also be profoundly affected by the limited flexibility of the brush polymer backbone as a result of the high steric hindrance between densely grafted side chains. On the other hand, the densely grafted side chains and extended conformation of brush polymers give them reduced entanglement density compared to their linear analogs. The reduced entanglement is a favorable feature to overcome the kinetic barrier for self-assembly, especially for ultrahigh MW polymers. Bowden and co-workers and Rzayev have recently found that

brush-coil and brush-brush block copolymers can self-assemble into exceptionally large structures with domain spacing above 100 nm.[10-12] Large domain structures are scientifically attractive and technically important with the potential to create periodic dielectric media to manipulate and control light, but have been challenging to achieve with linear block copolymers.[13-16] However, self-assembly of brush copolymers has been much less explored relative to the vast number of reports on their linear copolymer analogs.[10-12,17-18]

Well-defined macromolecular characteristics, such as the lengths of the backbone and side chains as well as the grafting density, are prerequisites to obtain ordered self-assembled structures. However, due to the complex architectures and demanding steric congestion, brush copolymers with controlled and high MW, low polydispersity (PDI), and complete side chain grafting remain challenging targets for polymer chemists. Current synthetic strategies to approach these targets normally involve multi-step reactions and separations.

The most explored method to make brush polymers is "graft from": the majority of previously reported brush block copolymers were synthesized by polymerizing different monomers from a diblock copolymer backbone using orthogonal polymerization mechanisms (i.e., radical polymerization and ring-opening polymerization).[10-12,19-20] To grow distinct side chains from a given backbone requires orthogonal polymerization mechanisms and/or selective protection/deprotection and subsequent functionalization of the copolymer backbone. Furthermore, the initiation efficiency of the macroinitiators may be limited,[12,21-22] and the monomer conversions must be kept low to avoid crosslinking due to the high density of initiating sites.[2,6-

[8,10-12,19-22] Alternatively, pre-formed side chains can be "grafted onto" a polymer backbone to prepare brush polymers.[23-25] Lanson et al. recently prepared brush block copolymers[23,26] and random copolymers[18] by grafting anionically prepared side chains onto polymers with pendent functional groups and by a combination of "graft from" and "graft onto" methods. However, purification to remove the unreacted side chains was required in each grafting step and repetitive protection and deprotection of the backbone functional groups was required to synthesize brush block copolymers.

On the other hand, the macromonomer (MM) approach toward brush copolymers is highly desirable,[27] because 1) it does not require orthogonal, non-interfering chemistry for grafting different side chains; 2) the side chain and the graft polymer can be well characterized; and 3) it is the only approach that guarantees complete grafting on every repeating unit. However, the macromonomer (MM) approach toward brush block copolymers is exceedingly challenging due to steric hindrance at the propagating polyMM chain end. Brush-coil block copolymers and brush random copolymers have been reported using uncontrolled metallocene-catalyzed[17] or radical[28] polymerizations and polycondensation[29] of MMs. As a result, the final graft polymers were polydisperse, and the MM conversion was limited. Neugebauer et al. reported copolymerization of MMs containing poly(ethylene oxide) and poly(dimethylsiloxane) or octadecane side chains by atom transfer radical polymerization (ATRP) to produce random or gradient brush copolymers depending on the relative polymerization rates of MMs.[30-31] However, the MMs used in those reports were relatively small and less hindered (MW≤1100) and no brush block copolymers were reported.

Chapter 4 described the highly efficient syntheses we developed for a variety of ultrahigh MW brush polymers with controlled MW (up to 2600 kg/mol) and very low PDI (1.01-1.07) using the highly active, fast-initiating Ru olefin metathesis catalyst $(H_2IMes)(pyr)_2(Cl)_2RuCHPh$ (**1**). Atomic force microscopy (AFM) revealed their rigid, wormlike structure and narrow PDI.[34]

In this chapter, we utilized ROMP of MMs to efficiently prepare a library of high MW, narrowly dispersed brush copolymers with different side chains, including brush block copolymers and brush random copolymers, each in one pot. ROMP of MMs allowed for facile control of the side chain and backbone block lengths and virtually arbitrary selection of side chains. In contrast to prior reports of ROMP synthesis of short graft block copolymers using molybdenum-based catalyst that were limited to oligomers with 5-10 side chains per "block" (starlike rather than brushlike architectures),[32,33] the present polymers have DP up to 200 per block. To the best of our knowledge, this report contains the first examples of high MW, narrowly dispersed brush block copolymers prepared sequentially via living polymerization of MMs.[35] The well-defined molecular characteristics of these brush copolymers provided an excellent model system to study the effect of side chain arrangement on the backbone and the relative ratio of the MMs on the self-assembly of brush copolymers. Specifically, we compared brush block copolymers (Figure 1 top) to brush random copolymers (Figure 1 bottom), showing that they provide convenient routes to self-assembled nanostructures with the backbone either predominantly orthogonal to the "intermaterial dividing surface"[36] or localized to the "intermaterial dividing surface," respectively.

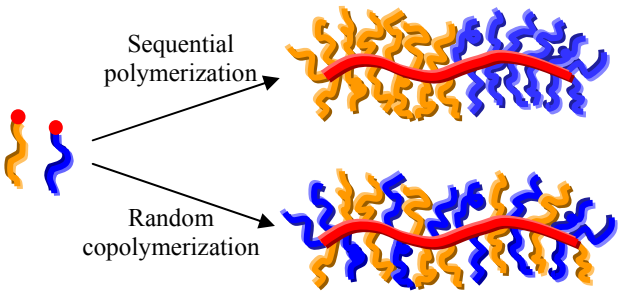

Figure 1. Schematic illustration of the synthesis of brush block copolymer through sequential addition (top) and brush random copolymer through random copolymerization (bottom) of MMs.

Results and Discussion

Syntheses of Brush Copolymers. We have synthesized ω-norbornenyl MMs containing poly(*n*-butyl acrylate) (P*n*BA), poly(*t*-butyl acrylate) (P*t*BA), and polystyrene (PS) side chains, as described in Chapter 4.[34] "Click" coupling of a norbornenyl group to the chain ends of polymers made by ATRP was used to prevent the unfavorable copolymerization of norbornene during ATRP.[37-38] ω-Norbornenyl MMs containing polylactide (PLA) side chains were also synthesized from ring-opening polymerization of D,L-lactide using a norbornenyl alcohol as the initiator and stannous octoate as the polymerization catalyst (Scheme 1). All MMs were narrowly dispersed. A high degree of norbornenyl end group functionalization was confirmed from good agreement between the degree of polymerization (DP) calculated by end group analysis using ^{1}H NMR spectroscopy (DP_{NMR}) and the DP calculated from the absolute MWs obtained from gel permeation chromatography (GPC) coupled with a multiangle laser light scattering (MALLS) detector (Table 1).

Scheme 1. Synthesis of macromonomers.[a]

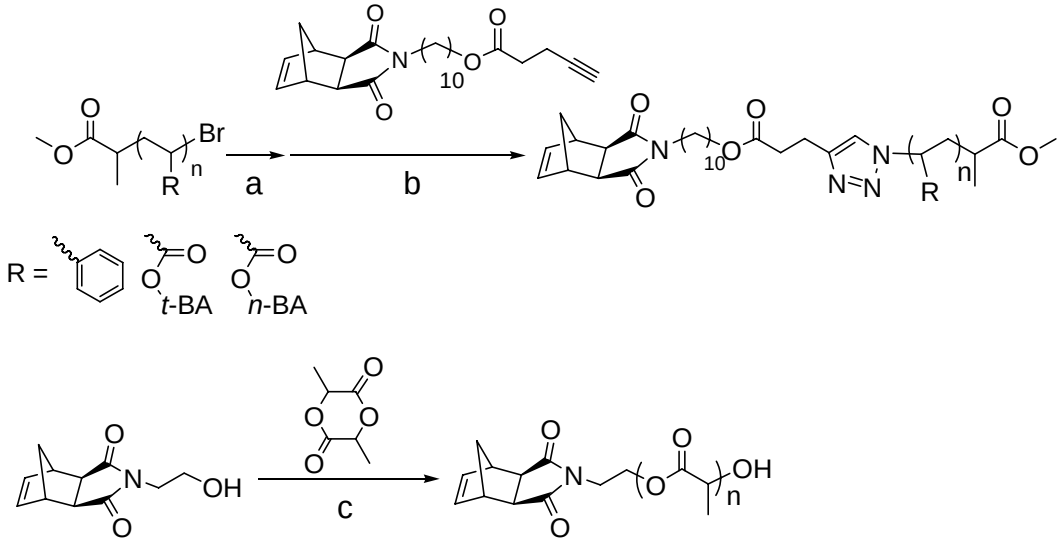

[a]Conditions: (a) NaN_3, DMF, 25 °C. (b) CuBr, PMDETA, THF, 50 °C. (c) $Sn[CH_3(CH_2)_3CH(C_2H_5)CO_2]_2$, 120 °C.

Table 1. Characteristics of *ω*-norbornenyl macromonomers and their polymerization rates

MM[a]	M_n[b] (kDa)	PDI[b]	DP_{NMR}[c]	DP_{GPC}[d]	k_p (min^{-1})[e]	$k_{p,rel}$[f]
NB(PS)6.6k	6.6	1.02	66	60	0.079	1
NB(PS)2.2k	2.2	1.03	19	17	0.092	1.2
NB(P*t*BA)4.7k	4.7	1.03	33	33	0.13	1.7
NB(PLA)7.0k	7.0	1.12	46	47	0.24	3.0
NB(PLA)4.7k	4.7	1.06	28	31	0.35	4.4
NB(P*n*BA)4.0k	4.0	1.06	29	28	0.33	4.2

[a]Macromonomers were named using a format of NB(X)Y, with X designating the type of prepolymer and Y designating the M_n of macromonomer. [b]Determined by GPC in THF using refractive index (RI) and MALLS detectors. [c]Calculated by comparing the integrations of the norbornenyl olefin and polymer backbone proton signals from ^1H NMR spectra in $CDCl_3$. [d]Calculated by (M_n – molar mass of norbornenyl end group) /

molar mass of monomer. [e]Conditions: $[MM]_0$ = 0.05M in THF at room temperature, $[MM/C]_0$ = 200. [f]$k_{p,\,rel}$ is the relative rate constant with respect to k_p of NB(PS)6.6k.

Polymerization of all these MMs using Ru catalyst **1** followed linear first-order kinetics (Figure 2A). GPC analyses of the polyMMs each showed narrow, monomodal peaks, and MWs increased linearly with conversion while the PDI remained less than 1.1 throughout the entire polymerization (Figure 2B). Furthermore, all MMs reached greater than 90% conversion within 1 h at room temperature. Although very weak signals that may correspond to MMs can be observed in the GPC traces of the crude polymer products, NMR spectroscopy of the reaction mixtures revealed the absence of the MM norbornene olefin signal. Therefore, the residual low MW peak may correspond to a small fraction of side chains with unfunctionalized chain ends in the MM. These observations collectively indicated the well-controlled character of ROMP of MMs and the extraordinary activity of catalyst **1**.

Due to the high activity of catalyst **1** and low critical monomer concentration of norbornene, the ROMP of MM can be performed at very low concentration ($[MM]_0$ = 0.05 M) to keep a relatively low viscosity of the solution throughout the polymerization. This is a distinct advantage over free radical polymerization of MMs.[39-42] Therefore, the polymerization is unlikely to be diffusion controlled (at least until the very late stage of the polymerization), in accord with the approximately linear first-order kinetics up to high conversions (>85%).

The polymerization rates, measured from the kinetic plot, depended weakly on both the MW and the structure of the MM (Table 1). In general, polyacrylate and polylactide MMs polymerized faster than polystyrene MMs. For example,

NB(PLA)7.0k polymerized about 3 times faster than NB(PS)6.6k despite their similar MW. The nature of the effects of side chain structure and MW on the polymerization rate of MMs warrants further investigation. It may be the local steric congestion around the propagating metallocycle or different solvent quality for various polymers that is causing the observed difference in the polymerization rate. Although the relative polymerization rates of different MMs varied less than an order of magnitude, they are significant when statistical copolymerization is attempted, since the relative polymerization rates can determine the distribution of side chains along the backbone (i.e., random vs. gradient).

(A)

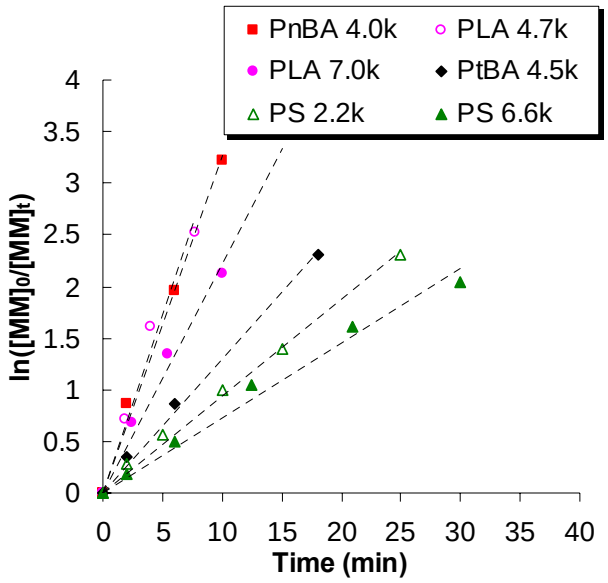

(B)

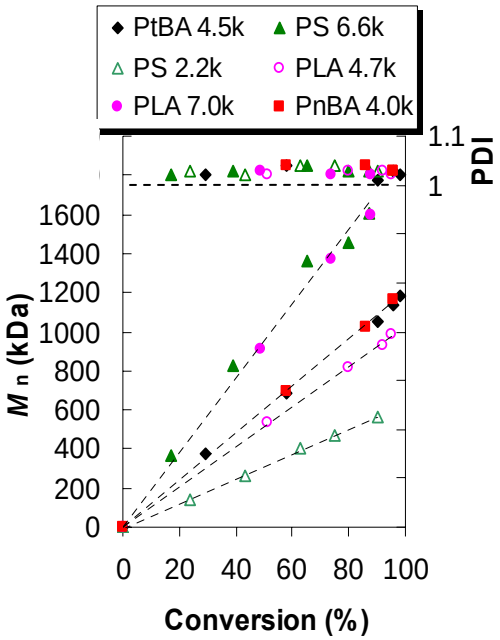

Figure 2. (A) Dependence of $\ln([MM]_0/[MM]_t)$ on time for ROMP of MMs. (B) Dependence of *M*n,GPC and PDI on conversion. Conditions: $[MM]_0$ = 0.05M in THF at room temperature, $[MM/C]_0$ = 200. The dashed lines are best-fit lines.

The controlled nature of the ROMP of MMs and the very high conversions motivated us to prepare brush block copolymers via simple sequential addition of MMs: Polymerization was initiated by injecting catalyst from a stock solution into a solution of the first type of MM at room temperature. As soon as the MM has been all consumed and only unfunctionalized side chains remained, a solution of a second type of MM was injected into the reaction mixture. GPC was used to analyze the reaction mixtures before the injection of the second MM and after completion of the second block polymerization. The GPC peak had shifted from the first block homopolymer to a shorter elution time corresponding to the brush diblock copolymer. The peak shape remained narrow without significant tailing, and the PDI remained low (≤1.10) (Figure 3). The low PDI was also indicated by the complete overlap of the light scattering trace and refractive index trace from GPC. Only very weak signal was

observed between 16 and 18 min in elution time, and this may correspond to unfunctionalized side chains in some of the MMs used. For example, in the brush PS and P*t*BA block copolymer, the intensity of the low MW peak remained similar in the first PS block and the diblock copolymer (Figure 3B), which may correspond to inert side chains in the PS MM. The order of addition of different MMs did not affect the MW or the PDI of the final block copolymers. Therefore, different MMs were arbitrarily polymerized sequentially to give various brush block copolymers, and the DP of each block was easily controlled by the ratio of MM to catalyst ([MM/C]). With narrow PDIs less than 1.1, regardless of the MW and combination of MMs, the MW of the copolymers measured by GPC-MALLS is close to or slightly higher than the theoretical MW. GPC analysis of the reaction mixture revealed the final conversions of MM to be greater than 90% in all the copolymerizations, while NMR spectroscopy showed no MM norbornene olefin signal.

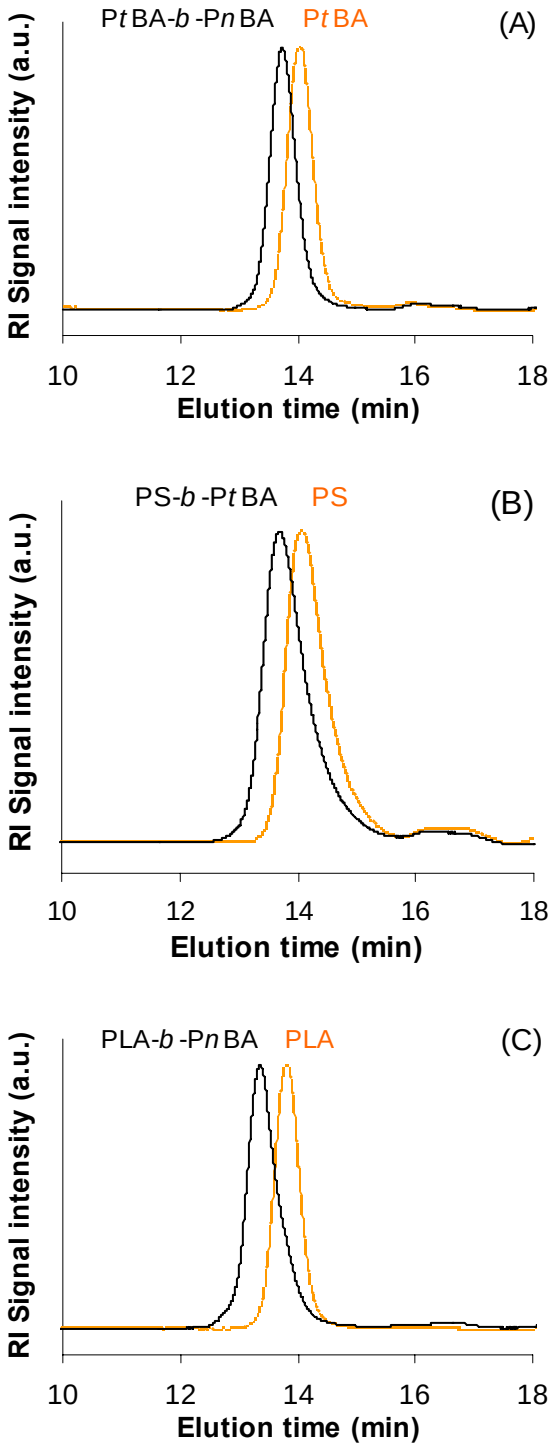

Figure 3. Representative GPC RI traces of the first block brush homopolymer (right) and the brush diblock copolymer (left) without any purification. (A) (PNB-*g*-P*t*BA)$_{100}$-*b*-(PNB-*g*-P*n*BA)$_{100}$; (B) (PNB-*g*-PS)$_{100}$-*b*-(PNB-*g*-P*t*BA)$_{50}$; (C) (PNB-*g*-PLA)$_{100}$-*b*-(PNB-*g*-P*n*BA)$_{100}$.

Table 2. Characteristics of brush copolymers

	MM_1	MM_2	Type	$[MM_1/C]$: $[MM_2/C]$[a]	Conv[b]	$M_{n,\,theo}$ (kDa)[c]	$M_{n,\,GPC}$ (kDa)[d]	PDI[d]
1	PS6.6k	P*n*BA4.0k	block	40:70	91%	540	730	1.04
2	PS6.6k	P*n*BA4.0k	block	40:200	91%	1060	1230	1.04
3	P*t*BA4.7k	P*n*BA4.0k	block	100:100	97%	870	890	1.05
4	P*t*BA4.7k	P*n*BA4.0k	block	100:200	98%	1270	1260	1.04
5	PS2.2k	P*t*BA4.7k	block	50:50	96%	345	340	1.03
6	PS2.2k	P*t*BA4.7k	block	100:50	94%	455	540	1.04
7	PLA4.7k	P*n*BA4.0k	block	20:180	98%	810	820	1.08
8	PLA4.7k	P*n*BA4.0k	block	40:160	97%	830	890	1.08
9	PLA4.7k	P*n*BA4.0k	block	100:100	97%	870	980	1.07
10	PLA4.7k	PnBA4.0k	block	200:200	96%	1740	1770	1.09
11	PLA4.7k	P*n*BA4.0k	random	50:50	98%	435	450	1.06
12	PLA4.7k	P*n*BA4.0k	random	100:100	97%	870	1050	1.05
13	PLA4.7k	P*n*BA4.0k	random	200:200	98%	1740	1880	1.10
14	PLA4.7k	P*n*BA4.0k	random	160:40	98%	910	1030	1.04
15	PLA4.7k	P*n*BA4.0k	random	130:70	98%	890	1030	1.05

[a] The ratio of each MM to Ru catalyst. [b] Conversion of MM to brush copolymer is determined by comparing the peak areas of brush copolymer and residual MM from GPC measurement of the final crude product without any purification. [c] $M_{n,\,theo} = M_{n,\,GPC}$ (MM_1) x $[MM_1/C]$ + $M_{n,\,GPC}$ (MM_2) x $[MM_2/C]$. [d] Determined by THF GPC using RI and MALLS detectors.

P*t*BA side chains in the brush block copolymers can be hydrolyzed into polyacrylic acid (PAA) using TFA in CH_2Cl_2, leaving the other block and the

backbone intact, as indicated by NMR spectroscopy. Thus, amphiphilic block brush copolymers were also easily obtained.

The side chain distribution along the brush copolymer backbone can dominantly affect the macromolecular packing in order to minimize the interfacial energy while retaining relatively extended backbone conformation. In this report, we focus on the study of the melt state self-assembly of copolymers containing PLA and P*n*BA side chains. We chose MMs NB(PLA)4.7k and NB(P*n*BA)4.0k as the side chains, because they possess very similar MWs and polymerization rates, and their copolymers can be thermally annealed relatively easily due to their low T_g's. These features allowed us to easily prepare a series of brush block and random copolymers with the same pair of side chains and matched backbone length, but varying the relative ratio of the two MMs (Table 2, entry 7-15). Brush block copolymers, *g*-[PLA_x-*b*-P*n*BA_y], with varied block lengths and ratios were synthesized via sequential addition of MMs. Brush random copolymers, *g*-[PLA_x-*ran*-P*n*BA_y], with varied total backbone length and side chain composition were synthesized via initiating a mixture of two MMs (Figure 3). Note that the subscripts x and y represent the number of side chains of each type—not the DP of the side chains, which was held fixed at approximately 30 for both the PLA and P*n*BA side chains (see the last two rows of Table 1). Since the ROMP of these MMs proceeded to very high conversions (>97%) and only a minute amount of catalyst was used (0.04-0.16 wt% to MMs used), no attempts to purify the polymer products were made. All polymer samples were simply dried under vacuum to remove solvent. These samples provided a model series to study how side chain distribution along the brush copolymer backbone affects brush

copolymer self-assembly in the melt state.

Thermal Analyses of Brush (Co)polymers. DSC analysis revealed the architectural effect of brush homopolymers and copolymers on the T_g of their side chains. For a PLA brush homopolymer (backbone DP=200) synthesized using NB(PLA)4.7k, a single thermal transition at 49 °C was observed in the temperature range of 0-200 °C scanned. This temperature corresponded to the T_g of amorphous PLA side chains and is close to the literature values. The T_g of the brush homopolymer was higher than that of the MM (42 °C), due to the increased MW and/or the increased molecular constraint resulting from linking the side chains along the formed polynorbornene backbone.[43] The T_g of PLA side chains in brush block copolymers was found to be about 49 °C, close to that of the PLA brush homopolymer, except for PLA_{20}-*b*-P*n*BA_{180} whose signal was too weak to enable accurate T_g determination (Table 3). This is consistent with phase separation in the block copolymers to form two distinct domains. In contrast, the T_g of PLA was found to be lower in the brush random copolymers, and increasing the P*n*BA content resulted in further suppression of the T_g of PLA. However, the T_g's of brush random copolymers were similar to that of the PLA MM, which indicated microphase separation of PLA and P*n*BA side chains. With equal amounts of PLA and P*n*BA in the brush random copolymers, the T_g was found to be 38 °C (Table 3). The lower T_g of PLA in random copolymers may be a result of smaller domain sizes than those in brush block copolymers.

Self-Assembly of Brush Copolymers in the Melt State. We investigated the self-assembly of brush copolymers in bulk using small angle X-ray scattering (SAXS) and in thin films using AFM. These two techniques provide complementary information

about the self-assembled morphology and domain spacing.

Brush random copolymers, *g*-[PLA-*ran*-P*n*BA], were thermally annealed at 100 °C for 12 h in order to achieve equilibrium, and prolonged annealing did not result in any further structural change. Brush random copolymers with an equal number of PLA and P*n*BA side chains (symmetric) exhibited a sharp principal SAXS peak at wavevector q^* along with peaks at integer multiples of q^* (Figure 4). This is indicative of a lamellar morphology, as expected due to the near symmetric volume fractions of the PLA and P*n*BA segments (f_{PLA} = 0.49). The domain spacing (d) calculated from q^* is very similar, 14.3 ± 0.3 nm, for all three symmetric random copolymers, independent of their backbone length. The independence of d-spacing on backbone length and the lamellar morphology suggest that the polynorbornene backbone is confined at the interface between PLA and P*n*BA layers, with the PLA and P*n*BA side chains segregated to opposite sides of the brush polymer backbone to minimize contact between dissimilar chains.

Furthermore, as the symmetric random copolymers were heated, they underwent a transition from an ordered lamellar phase into a microphase disordered regime. The order-disorder transition (ODT) temperature, T_{ODT}, can be evaluated using the discontinuity in the plot of inverse primary peak intensity vs inverse temperature (Figure 5), using SAXS patterns acquired in 5 °C step ramping with 5 min thermal equilibration at each temperature. This was accompanied by the disappearance of higher order peaks. The T_{ODT} was found to hardly change, giving 75-85 °C for *g*-[PLA_{50}-*ran*-P*n*BA_{50}], *g*-[PLA_{100}-*ran*-P*n*BA_{100}], and *g*-[PLA_{200}-*ran*-P*n*BA_{200}] as the MW increased from 450 to 1880 kDa. The broad scattering peak in

SAXS that remained above the ODT originated from intramolecular correlations of block copolymers.[44] For a wide range of block copolymers, T_{ODT} is controlled by the product of the Flory-Huggins interaction parameter χ and the total degree of polymerization N.[44] The similar T_{ODT}'s observed for the brush random copolymers over a wide range of the brush backbone length suggested that the degree of polymerization N of the side chains dictates the T_{ODT}. This is consistent with side chain microphase separation with the backbones localized at interfaces between PLA and P*n*BA domains (Figure 6 top).

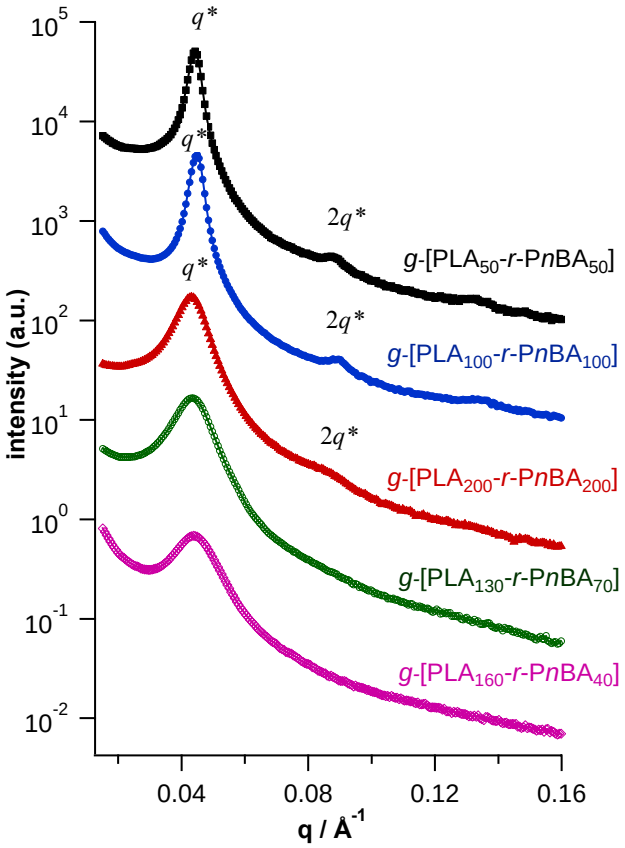

Figure 4. SAXS curves for brush random copolymers, *g*-[PLA-*ran*-P*n*BA].

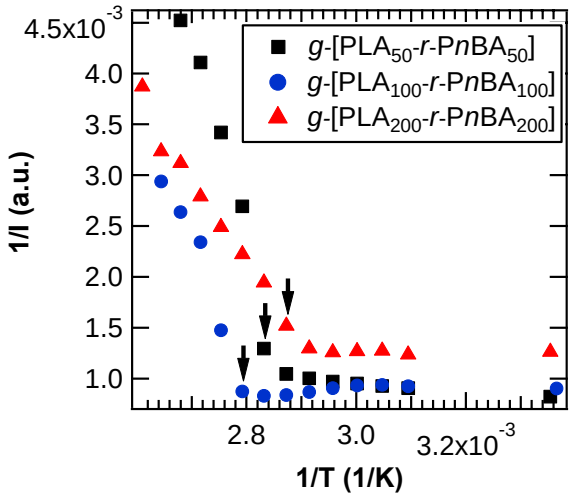

Figure 5. Inverse intensity of peak heights in the vicinity of the order-disorder transition for brush random copolymers, *g*-[PLA-*ran*-P*n*BA]. The arrows mark the T_{ODT}'s.

We studied the morphology of brush random copolymers in thin films using AFM. Based on the T_{ODT} determined using SAXS, these samples were annealed at 70 °C, which is below the T_{ODT} but still above the T_g of PLA. AFM showed that the films were featureless before annealing (Figure 7a). After annealing, a layer of islands with very uniform height was clearly observed for each of the symmetric random copolymers (Figure 7b-d). An island layer is formed if the natural repeat spacing of a parallel oriented block copolymer is incommensurate with the film thickness, and the film segregates excess material to the top surface to form an incomplete layer.[45-47] The height difference between the thicker and thinner regions of the film is equal to the natural period of the block copolymer. Here the island layers are remarkably uniform across areas of tens of micrometers, with thickness of 17-20 nm for all three samples. The height values are very close to the bulk *d*-spacings measured by SAXS, indicating that the domain spacing of parallel oriented lamellae in the film is similar to domain spacing in the bulk.

Table 3. Molecular and Morphological Characteristics of PLA-P*n*BA Brush Random and Block Copolymers

	f_{PLA}[a]	$T_{g,\ PLA}$/°C[b]	*d* (SAXS)/nm[c]	*d* (AFM)/nm[d]	T_{ODT}/°C[e]
g-[PLA_{50}-*ran*-$PnBA_{50}$]	0.49	38	14.2	18	80
g-[PLA_{100}-*ran*-$PnBA_{100}$]	0.49	38	14.0	21	85
g-[PLA_{200}-*ran*-$PnBA_{200}$]	0.49	38	14.6	17	75
g-[PLA_{130}-*ran*-$PnBA_{70}$]	0.63	39	-	-	-
g-[PLA_{160}-*ran*-$PnBA_{40}$]	0.79	42	-	-	-
g-[PLA_{100}-*b*-$PnBA_{100}$]	0.49	49	116	-	-
g-[PLA_{40}-*b*-$PnBA_{160}$]	0.19	49	-	-	-
g-[PLA_{20}-*b*-$PnBA_{180}$]	0.09	-	64	-	-

[a]volume fraction of PLA calculated using densities ρ_{PnBA} = 0.99 g/mL, ρ_{PLA} = 1.25 g/mL. [b]T_g of PLA side chain, measured by DSC with heating rate of 15 °C/min. [c]Domain spacing determined by SAXS. [d]Lamellar thickness determined by AFM cross-sectional analysis. [e]Order-disorder transition temperature determined by SAXS.

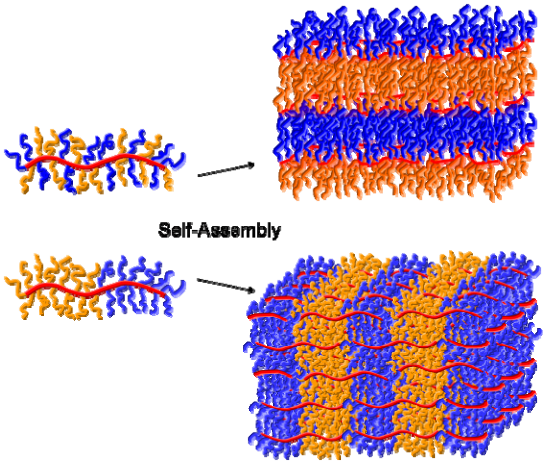

Figure 6. Proposed assembly of symmetric brush random copolymer and block copolymer.

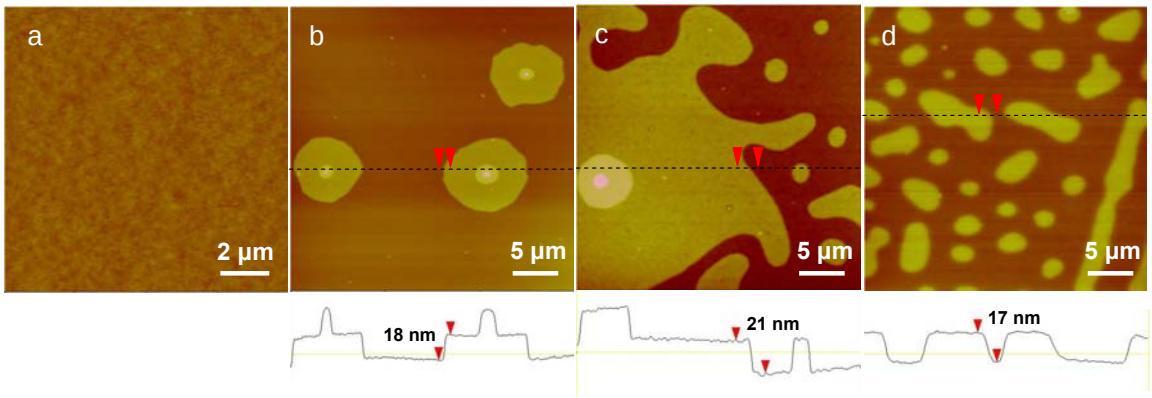

Figure 7. AFM height images of brush random copolymer thin films (120-150 nm) on silicon wafer and their cross-sectional analysis. (a) *g*-[PLA_{100}-*ran*-P*n*BA_{100}] as cast, and after annealing (b) *g*-[PLA_{50}-*ran*-P*n*BA_{50}], (c) *g*-[PLA_{100}-*ran*-P*n*BA_{100}], (d) *g*-[PLA_{200}-*ran*-P*n*BA_{200}]. The vertical scale is 30 nm for (a) and 100 nm for (b)-(d).

Due to the independence of lamellar thickness on brush polymer MW, we propose that uniform lamellar structures can be obtained using polydisperse brush copolymer samples. Indeed, an indistinguishable "islands and holes" morphology with 17-20 nm in height was obtained from blends of any two of the symmetric random copolymers at arbitrary ratios after annealing (Figure 8). This further supports the complete dominance of the side chains in governing the self-assembly of these brush random copolymers.

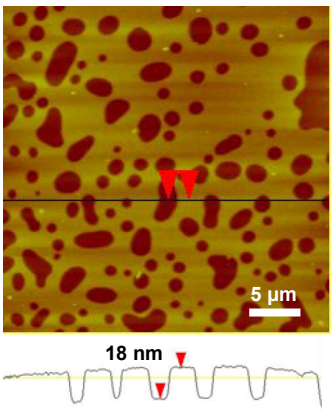

Figure 8. AFM height image of thin films of a mixture of two brush random copolymers, $(PNB\text{-}g\text{-}PLA)_{50}$-*ran*-$(PNB\text{-}g\text{-}PnBA)_{50}$ and $(PNB\text{-}g\text{-}PLA)_{100}$-*ran*-$(PNB\text{-}g\text{-}PnBA)_{100}$ (1:1), and its cross-sectional analysis. A hole layer was formed in this case.

In contrast to the symmetric random copolymers, when PLA and P*n*BA side chains were incorporated in uneven amounts (Table 2, entry 14 and 15), microphase separation of the side chains was not observed: No structural features were observed in thin films by AFM after extensive annealing at temperatures ranging from 75 to 140 °C. SAXS of *g*-[PLA_{160}-*ran*-P*n*BA_{40}] and *g*-[PLA_{130}-*ran*-P*n*BA_{70}] showed only one broad peak with no higher-order peaks; the single peak corresponds to intramolecular correlations between side chains of the block copolymers. Furthermore, the peak intensity continuously decreased upon heating, and no ODT was observed (Figure 9). As the side chains microphase separate to opposite sides of the backbone, the resulting asymmetric space filling on the backbone makes it impossible to assemble into lamellae. Meanwhile, the backbone of a brush polymer may be more difficult to coil than a linear polymer to adopt other morphologies, as a result of the high congestion of the segregated side chains.

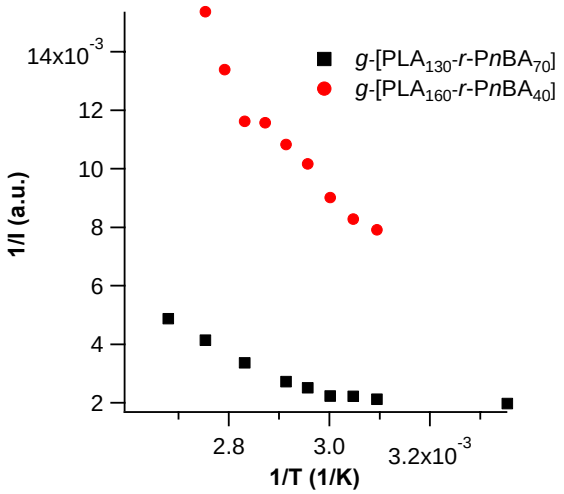

Figure 9. Inverse intensity of peak heights vs inverse temperature for asymmetric brush random copolymers.

We next investigated the self-assembly of brush block copolymers, *g*-[PLA-*b*-P*n*BA]. Due to the very large domain spacing in the assembled brush block

copolymers, principal q^* was out of the q range obtainable by SAXS in some samples (Figure 10). For the symmetric block copolymers, *g*-[PLA_{50}-*b*-P*n*BA_{50}] showed very sharp principal q^* and evenly spaced odd-order scattering peaks, and the even-order peaks were significantly suppressed. This scattering pattern strongly indicated symmetric lamellar morphology with a *d*-spacing of 50 nm. As the MW doubles, *g*-[PLA_{100}-*b*-P*n*BA_{100}] clearly showed multiple higher-order scattering peaks up to the 12th order. The even distribution of scattering peaks to $12q^*$ indicated remarkably well-ordered lamellar morphology with a *d*-spacing of 116 nm, consistent with the fact that principal q^* was out of the q range obtainable by SAXS. This length scale is close to the fully extended length of a polynorbornene brush homopolymer with backbone DP = 220 and PS side chains of 6.6 kDa, as previously observed by AFM.[34] Although clear AFM imaging of individual *g*-[PLA_{100}-*b*-P*n*BA_{100}] polymers has been difficult due to the aggregation of molecules, AFM revealed wormlike shapes with contour lengths of ca 110-130 nm for a PLA brush homopolymer with backbone DP = 200 prepared using the same MM as in the block copolymer (Figure 9a). Therefore, the large lamellar *d*-spacing of *g*-[PLA_{100}-*b*-P*n*BA_{100}] is dictated by the length of its highly extended polynorbornene backbone and suggests interdigitated packing of the molecules in the lamellae (Figure 6 bottom). This is further supported by the the almost linear increase of *d*-spacing from 50 to 116 nm, when the MW doubles from that of *g*-[PLA_{50}-*b*-P*n*BA_{50}] to that of *g*-[PLA_{100}-*b*-P*n*BA_{100}]. Notably, the largest symmetric block copolymer *g*-[PLA_{200}-*b*-P*n*BA_{200}] (Table 2, entry 10) appeared green spontaneously upon slowly evaporating the solvent (Figure 13). This indicates that the domain spacing in this ultrahigh MW sample is large enough to reflect green light.[48]

However, only some very low intensity SAXS peaks were observed for *g*-[PLA_{200}-*b*-P*n*BA_{200}] and *d*-spacing cannot be calculated. This is because the high-intensity lower-order scattering peaks were out of the range of the SAXS used due to the very large domain size in this sample. Ultrasmall angle X-ray scattering (USAXS) needs to be used in the future to study the brush polymer assembly pocessing large domain sizes (>100 nm).

On the other hand, highly asymmetric block copolymers, *g*-[PLA_{20}-*b*-P*n*BA_{180}] and *g*-[PLA_{40}-*b*-P*n*BA_{160}], formed non-lamellar morphologies. Both materials showed scattering peaks at very low *q*, a feature indicative of microphase separation, with *q** inaccessible for *g*-[PLA_{40}-*b*-P*n*BA_{160}] and *q** corresponding to a domain spacing of 64 nm for *g*-[PLA_{20}-*b*-P*n*BA_{180}] (Figure 11). Based on the domain spacing for *g*-[PLA_{20}-*b*-P*n*BA_{180}], it is clear that the backbone is not fully extended in its highly asymmetric polymer. In addition, both polymers show oscillations at higher *q* that originate from the form factor of the block copolymer aggregates.[49] Although the quality of fits is not sufficient to identify the specific shape of the aggregates, the period of the oscillations allows us to identify the characteristic size of the presumably spherical or cylindrical PLA domains with sizes of 38 and 67 nm in diameter, respectively, irregularly distributed in a matrix of P*n*BA. In addition, the PLA domain size is consistent with the calculated result using the domain spacing of 64 nm obtained from *q** and 9% PLA volume fraction in *g*-[PLA_{20}-*b*-P*n*BA_{180}]. The non-lamellar morphologies formed from these asymmetric brush block copolymers suggest that the backbone is not as fully extended as in the symmetric brush block copolymer, *g*-[PLA_{100}-*b*-P*n*BA_{100}]. On the other hand, the decreased ordering in

asymmetric block copolymers suggests frustrated packing when the backbone has to adopt non-lamellar morphologies due to its reduced flexibility. Similar packing frustration has also been suggested for asymmetric brush block copolymers with side chains of different MWs.[12]

Thin films of the block copolymer *g*-[PLA_{100}-*b*-P*n*BA_{100}] after spin-coating from toluene solution showed large cylindrical micellar structures of 200 nm wide and several micrometers long as imaged by AFM (Figure 12b), in sharp contrast to the featureless as-cast film from the random copolymer, *g*-[PLA_{100}-*ran*-P*n*BA_{100}], at the same MW and composition. After annealing, the surface topology became rough, but clear phase separation was observed from the sharp contrast in the phase image, which derives from mechanical property differences between the PLA and P*n*BA blocks in the copolymers. Microphase separation in thin films of the asymmetric brush block copolymers was also observed from the AFM phase images. However, the structural assignment for the thin film morphologies of these brush block copolymers was unclear. This is because the film thickness is similar to the polymer domain spacing in bulk and corresponds to one layer of molecular packing. Therefore, the surface effect on the thin film morphology makes it difficult to correlate to the bulk morphology for large brush block copolymers.

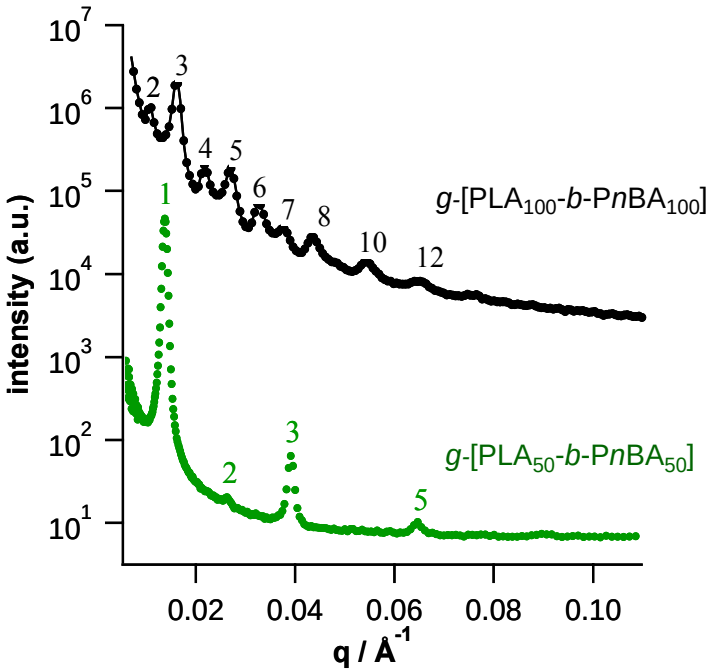

Figure 10. SAXS curves for symmetric brush block copolymers, *g*-[PLA-*b*-P*n*BA].

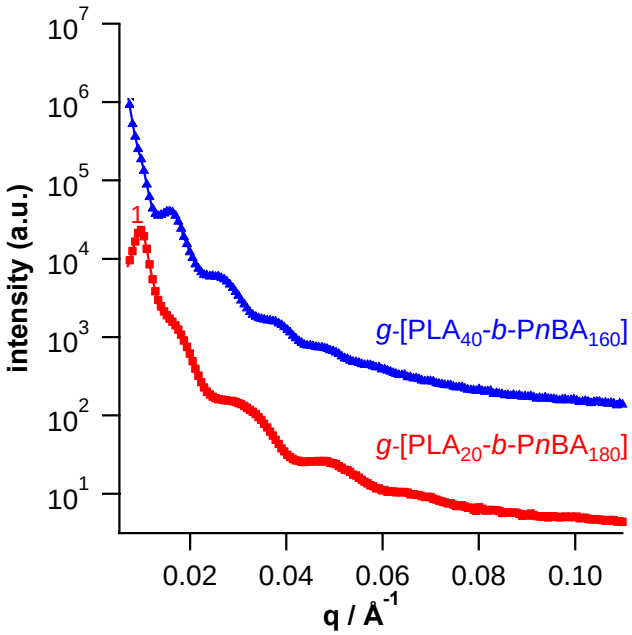

Figure 11. SAXS curves for asymmetric brush block copolymers, *g*-[PLA-*b*-P*n*BA].

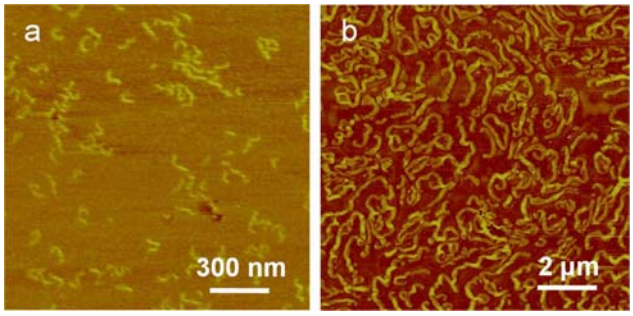

Figure 12. AFM phase images of (a) individual PLA brush homopolymers ($DP_{backbone}$ = 200, MM NB(PLA)4.7k was used) on mica; (b) brush block copolymer, *g*-[PLA_{100}-*b*-P*n*BA_{100}], morphology in thin film (ca 120 nm) as cast from 2.5% toluene solution onto silicon wafer.

Figure 13. Photograph of slowly dried *g*-[PLA_{200}-*b*-P*n*BA_{200}] (Table 2, entry 10) showing green color due to reflectance from the large self-assembled domains.

Conclusions

ROMP of various MMs bearing polyacrylate, polystyrene, and polylactide chains using highly active, fast initiating Ru catalyst has shown typical characteristics of a living polymerization, such as first-order kinetics and linear MW growth with increasing conversion. The living nature of ROMP and very high conversion (>90%) of MMs have allowed facile one-pot preparation of a variety of high MW narrowly dispersed brush block and random copolymers in high conversions, which otherwise involve multiple steps to synthesize using different grafting techniques. The length of each block and the overall backbone can be easily controlled by the ratio of MM to catalyst.

By choosing MMs with the similar polymerization rates, we prepared a series of brush block and random copolymers from a pair of MMs, NB(PLA)4.7k and NB(P*n*BA)4.0k, varying their relative ratios. In symmetric brush random copolymers (equal number of PLA and P*n*BA side chains), the side chains were found to microphase separate into lamellar morphology with domain spacing of about 14 nm as determined by SAXS. AFM studies of thin film samples also revealed lamellar structures with similar thickness of 17-21 nm. The domain spacing and T_{ODT} were insensitive to the brush copolymer backbone length, suggesting microphase separation of side chains to opposite sides of the brush polymer backbone and that the side chains played a dominant role in the self-assembly. On the other hand, the brush block copolymer with the same number of PLA and P*n*BA side chains self-assembled into highly ordered, large lamellar domains over 100 nm as revealed by SAXS. The domain size was dictated by the backbone length. The regular, spontaneous, large assembly of brush block copolymers makes them ideal polymer materials for single-component photonic crystals, which are important for advanced optical applications.

Asymmetric brush copolymers containing different numbers of two types of side chains did not form well-ordered morphologies. This may be attributed to the reduced backbone flexibility of brush polymers and their increased difficulty to adopt coiled conformations.

Controlled ROMP of MMs greatly simplifies the syntheses of brush copolymers. The combination of facile synthesis and good structural control of brush copolymers with the functional group tolerant Ru catalyst opens the door to further studies of the self-assembly of these macromolecular architectures. Brush copolymers provide a unique

macromolecular platform for bottom-up assembly to form nanostructures with large domain spacings and controlled intermaterial dividing surfaces.

Experimental Section

Materials. The synthesis and characterization of PMA, P*t*BA, and PS MMs have been described in Chapter 4 and the P*n*BA MM was synthesized in a similar manner. *n*-BA was passed through a column of basic alumina immediately before use. D, L-lactide was recrystallized from ethyl acetate three times. All other materials were obtained from commercial sources and used as received.

Synthesis of PLA macromonomers. A flame-dried Schlenk tube was charged with N-(hydroxyethyl)-*cis*-5-norbornene-exo-2,3-dicarboximide (54 mg, 0.26 mmol), D, L-lactide (1.5 g, 10.4 mmol), tin (II) 2-ethylhexanoate (2.1 mg, 5.2 μmol), and a stir bar. The tube was evacuated and backfilled with argon four times, and was then immersed in an oil bath at 120 °C. After 4 h, the contents were cooled to room temperature, diluted with dichloromethane, and precipitated into acidic methanol. The MM was isolated by decanting the supernatant and drying *in vacuo*. ^{1}H NMR (500 MHz, $CDCl_3$): δ 1.24 (br d, 1H), 1.40-1.70 (br, 253H), 2.72 (br, 2H), 3.28 (br, 2H), 3.70-3.85 (m, 2H), 4.22-4.40 (m, 3H), 5.00-5.30 (m, 84H), 6.30 (br t, 2H). GPC-MALLS: M_n = 7.0 kg/mol, M_w/M_n = 1.12.

General procedure for synthesis of brush block and random copolymers via ROMP of macromonomers. An oven-dried vial was charged with 100 mg MM for the first block and a stir bar. The vial was then degassed, and the desired amount of degassed anhydrous THF ($[M]_0$ = 0.05-0.10 M) was added via syringe under an argon atmosphere to dissolve the MM. A stock solution of Ru catalyst in degassed anhydrous THF was prepared in a separate vial. The desired amount of catalyst was injected into the MM

solution to initiate the polymerization. The reaction was allowed to proceed at room temperature for 20-30 min. After the first polymerization was complete, the desired amount of second MM was added as a solution in THF ($[M]_0$ = 0.05-0.10 M). After 1 h, the reaction mixture was quenched with one drop of ethyl vinyl ether. A sample was then withdrawn for GPC analysis without any purification. The block copolymer was isolated either by precipitating into cold methanol, or by simply drying *in vacuo.*

The random copolymers were synthesized using a similar procedure as the block copolymers, except that two types of MMs were added together in the reaction vial before catalyst injection.

Characterization. *^1H and ^{13}C NMR spectroscopy* was recorded in $CDCl_3$ or DMF-*d*7 using a Varian Mercury 300 or Varian Inova 500 spectrometer. Chemical shifts (δ) are expressed in ppm downfield from tetramethylsilane using the residual protiated solvent signal as an internal standard.

Gel permeation chromatography (GPC) was carried out in THF on two PLgel 10 μm mixed-B LS columns (Polymer Laboratories) connected in series with a DAWN EOS multiangle laser light scattering (MALLS) detector and an Optilab DSP differential refractometer (both from Wyatt Technology). No calibration standards were used, and d*n*/d*c* values were obtained for each injection by assuming 100% mass elution from the columns.

Atomic force microscopy (AFM) images were taken using a Nanoscope IV Scanning Probe Microscope Controller (Digital Instruments, Veeco Metrology Group) in tapping mode in air at room temperature using silicon tips (spring constant = 40-50 N/m, resonance frequency = 170-190 kHz, and tip radius of curvature <10 nm). The samples

for imaging individual polymers were prepared by spin casting very dilute solutions (<0.01 wt%) in chloroform onto freshly cleaved mica at 1500 rpm. Thin film samples were prepared by spin casting solutions (2.5 wt%) in toluene onto Si(100) with a native oxide layer at 1500 rpm. A Gartner L116-C ellipsometer was used to measure the film thickness.

Differential scanning calorimetry (DSC) was performed on a Perkin-Elmer DSC 7. Samples were heated to 180 °C at 20 °C/min to erase any thermal history, then cooled to 0 °C at 20 °C/min, and reheated to 150 °C at 15 °C/min. The second heating scan was used to determine the T_g of PLA.

Small angle X-ray scattering (SAXS). Samples for SAXS were prepared by annealing polymers in vacuum (10 mTorr) at 110 °C for 12 h to form 1 mm thick disks and then sealing the samples between Kapton windows. Experiments were performed on beamline 27X-C at Brookhaven National Lab. The beamline was configured with an X-ray wavelength of 1.371 Å. Samples were corrected for transmission, thickness, empty cell, and dark field scattering and radially averaged to produce 1 dimensional I vs. q plots. Temperature-dependent experiments were conducted by increasing temperature in 5 °C steps with 5 min of thermal equilibration after reaching each temperature before starting data acquisition.

References

(1) (a) Sheiko, S. S.; Möller, M. *Chem. Rev.* **2001**, *101*, 4099-4124. (b) Hadjichristidis, N. P., M.; Pispas, S.; Iatrou, H. *Chem. Rev.* **2001**, *101*, 3747-3792. (c) Zhang, M.; Müller, A. H. E. *J. Polym. Sci., Part A: Polym. Chem.* **2005**, *43*, 3461-3481.

(2) Li, C.; Gunari, N.; Fischer, K.; Janshoff, A.; Schmidt, M. *Angew. Chem. Int. Ed.* **2004**, *43*, 1101-1104.

(3) Djalali, R.; Li, S.-Y.; Schmidt, M. *Macromolecules* **2002**, *35*, 4282-4288.

(4) Zhang, M.; Drechsler, M.; Müller, A. H. E. *Chem. Mater.* **2004**, *16*, 537-543.

(5) Zhang, M.; Estournes, C.; Bietsch, W.; Müller, A. H. E. *Adv. Funct. Mater.* **2004**, *14*, 871-882.

(6) Cheng, C.; Qi, K.; Khoshdel, E.; Wooley, K. L. *J. Am. Chem. Soc.* **2006**, *128*, 6808-6809.

(7) Huang, K.; Rzayev, J. *J. Am. Chem. Soc.* **2009**, *131*, 6880-6885.

(8) Tang, C.; Dufour, B.; Kowalewski, T.; Matyjaszewski, K. *Macromolecules* **2007**, *40*, 6199-6205.

(9) (a) Bates, F. S.; Fredrickson, G. H. *Phys. Today* **1999**, *52*, 32-38. (b) Klok, H.-A.; Lecommandoux, S. *Adv. Mater.* **2001**, *13*, 1217-1229. (c) Discher, D. E.; Eisenberg, A. *Science* **2002**, *297*, 967-973. (d) Hamley, I. W. *Angew. Chem. Int. Ed.* **2003**, *42*, 1692-1712. (e) Hadjichristidis, N.; Iatrou, H.; Pitsikalis, M.; Pispas, S.; Avgeropoulos, A. *Prog. Polym. Sci.* **2005**, *30*, 725-782. (f) Ruzette, A.-V.; Leibler, L. *Nat. Mater.* **2005**, *4*, 19-31. (g) Cheng, J. Y.; Ross, C. A.; Smith, H. I.; Thomas, E. L. *Adv. Mater.* **2006**, *18*, 2505-2521. (h) Cui, H.; Chen, Z.; Zhong, S.; Wooley, K. L.; Pochan, D. J. *Science* **2007**, *317*, 647-650. (i) Tang, C.; Lennon, E. M.; Fredrickson, G. H.; Kramer, E. J.; Hawker, C. J. *Science* **2008**, *322*, 429-432.

(10) Runge, M. B.; Bowden, N. B. *J. Am. Chem. Soc.* **2007**, *129*, 10551-10560.

(11) Runge, M. B.; Lipscomb, C. E.; Ditzler, L. R.; Mahanthappa, M. K.; Tivanski, A. V.; Bowden, N. B. *Macromolecules* **2008**, *41*, 7687-7694.

(12) Rzayev, J. *Macromolecules* **2009**, *42*, 2135-2141.

(13) Joannopoulos, J. D.; Meade, R. D.; Winn, J. N. *Photonic Crystals*, Princeton University Press, 1995.

(14) Edrington, A. C.; Urbas, A. M.; DeRege, P.; Chen, C. X.; Swager, T. M.; Hadjichristidis, N.; Xenidou, M.; Fetters, L. J.; Joannopoulos, J. D.; Fink, Y.; Thomas, E. L. *Adv. Mater.* **2001**, *13*, 421-425.

(15) Park, C.; Yoon, J.; Thomas, E. L. *Polymer* **2003**, *44*, 6725-6760.

(16) Kang, Y.; Walish, J. J.; Gorishnyy, T.; Thomas, E. L. *Nat. Mater.* **2007**, *6*, 957-960.

(17) Neiser, M. W.; Muth, S.; Kolb, U.; Harris, J. R.; Okuda, J.; Schmidt, M. *Angew. Chem. Int. Ed.* **2004**, *43*, 3192-3195.

(18) Lanson, D.; Ariura, F.; Schappacher, M.; Borsali, R.; Deffieux, A. *Macromolecules* **2009**, *42*, 3942-3950.

(19) Runge, M. B.; Dutta, S.; Bowden, N. B. *Macromolecules* **2006**, *39*, 498-508.

(20) Lee, H.-I.; Matyjaszewski, K.; Yu-Su, S.; Sheiko, S. S. *Macromolecules* **2008**, *41*, 6073-6080.

(21) Neugebauer, D.; Sumerlin, B. S.; Matyjaszewski, K.; Goodhart, B.; Sheiko, S. S. *Polymer* **2004**, *45*, 8173-8179.

(22) Sumerlin, B. S.; Neugebauer, D.; Matyjaszewski, K. *Macromolecules* **2005**, *38*, 702-708.

(23) Lanson, D.; Schappacher, M.; Borsali, R.; Deffieux, A. *Macromolecules* **2007**, *40*, 5559-5565.

(24) Schappacher, M.; Deffieux, A. *Macromolecules* **2005**, *38*, 7209-7213.

(25) Gao, H.; Matyjaszewski, K. *J. Am. Chem. Soc.* **2007**, *129*, 6633-6639.

(26) Lanson, D.; Schappacher, M.; Borsali, R.; Deffieux, A. *Macromolecules* **2007**, *40*, 9503-9509.

(27) Hadjichristidis, N.; Pitsikalis, M.; Iatrou, H.; Pispas, S. *Macromol. Rapid Commun.* **2003**, *24*, 979-1013.

(28) Stephan, T.; Muth, S.; Schmidt, M. *Macromolecules* **2002**, *35*, 9857-9860.

(29) Deimede, V.; Kallitsis, J. K. *Chem.-Eur. J.* **2002**, *8*, 467-473.

(30) Neugebauer, D.; Zhang, Y.; Pakula, T.; Matyjaszewski, K. *Macromolecules* **2005**, *38*, 8687-8693.

(31) Neugebauer, D.; Theis, M.; Pakula, T.; Wegner, G.; Matyjaszewski, K. *Macromolecules* **2006**, *39*, 584-593.

(32) Heroguez, V.; Gnanou, Y.; Fontanille, M. *Macromolecules* **1997**, *30*, 4791-4798.

(33) Nomura, K.; Takahashi, S.; Imanishi, Y. *Macromolecules* **2001**, *34*, 4712-4723.

(34) Xia, Y.; Kornfield, J. A.; Grubbs, R. H. *Macromolecules* **2009**, *42*, 3761-3766.

(35) Karen L. Wooley and co-workers reported the synthesis of brush block copolymers using similar strategy soon after our initial report: Li, Z.; Ma, J.; Cheng, C.; Zhang, K.; Wooley, K. L. *Macromolecules* **2010**, *43*, 1182-1184.

(36) Winey, K. I.; Thomas, E. L.; Fetters, L. J. *J. Chem. Phys.* **1991**, *95*, 9367-9375.

(37) Cheng, C.; Khoshdel, E.; Wooley, K. L. *Macromolecules* **2005**, *38*, 9455-9465.

(38) Patton, D. L.; Advincula, R. C. *Macromolecules* **2006**, *39*, 8674-8683.

(39) Tsukahara, Y. T., K.;Yamashita, Y.;Shimada, S. *Macromolecules* **1990**, *23*, 5201-5208.

(40) Dziezok, P.; Sheiko, S. S.; Fischer, K.; Schmidt, M.; Möller, M. *Angew. Chem. Int. Ed.* **1997**, *36*, 2812-2815.

(41) Roos, S. G.; Müller, A. H. E.; Matyjaszewski, K. *Macromolecules* **1999**, *32*, 8331-8335.

(42) Shinoda, H.; Matyjaszewski, K. *Macromolecules* **2001**, *34*, 6243-6248.

(43) Fox, T. G.; Flory, P. J. *J. Polym. Sci.* **1954**, *14*, 315.

(44) Leibler, L. *Macromolecules* **1980**, *13*, 1602-1617.

(45) Coulon, G.; Collin, B.; Ausserre, D.; Chatenay, D.; Russell, T. P. *J. Phys. (Paris)* **1990**, *51*, 2801-2811.

(46) Mayes, A. M.; Russell, T. P.; Bassereau, P.; Baker, S. M.; Smith, G. S. *Macromolecules* **1994**, *27*, 749-755.

(47) Olsen, B. D.; Li, X.; Wang, J.; Segalman, R. A. *Macromolecules* **2007**, *40*, 3287-3295.

(48) The wavelength of the reflected light at the interfaces of multilayer lamellae is governed by: $\lambda = 2(n_1d_1 + n_2d_2)$, where n and d are the refractive index and the thickness of each layer. In a rough estimate, taking $n_1 = n_2 = 1.5$ for both polymer layers and $\lambda = 500$ nm for green light, the domain spacing is calculated to be about 170 nm for a symmetric lamellar morphology presumably formed in the symmetric block copolymer *g*-[PLA_{200}-*b*-P*n*BA_{200}].

(49) Kinning, D. J.; Thomas, E. L. *Macromolecules* **1984**, *17*, 1712-1718.